2022-03

Subaerial-submarine morphological changes at Stromboli volcano (Italy) induced by the 20192020 eruptive activity

Di Traglia, F

10.1016/j.geomorph.2021.108093
Geomorphology
Elsevier

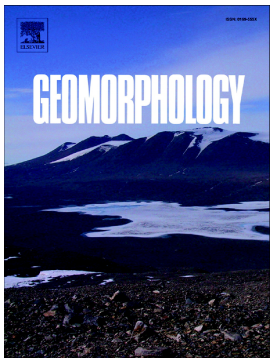

Subaerial-submarine morphological changes at Stromboli volcano (Italy) induced by the 2019–2020 eruptive activity

Federico Di Traglia, Alessandro Fornaciai, Daniele Casalbore, Massimiliano Favalli, Irene Manzella, Claudia Romagnoli, Francesco Latino Chiocci, Paul Cole, Teresa Nolesini, Nicola Casagli

PII: S0169-555X(21)00501-8

DOI: https://doi.org/10.1016/j.geomorph.2021.108093

Reference: GEOMOR 108093

To appear in: *Geomorphology*

Received date: 3 October 2021

Revised date: 20 December 2021

Accepted date: 20 December 2021

Please cite this article as: F. Di Traglia, A. Fornaciai, D. Casalbore, et al., Subaerial-submarine morphological changes at Stromboli volcano (Italy) induced by the 2019–2020 eruptive activity, *Geomorphology* (2021), https://doi.org/10.1016/j.geomorph.2021.108093

Subaerial-submarine morphological changes at Stromboli volcano (Italy) induced by the 2019-2020 eruptive activity

Federico Di Traglia[1]*, Alessandro Fornaciai[2], Daniele Casalbore[3,4], Massimiliano Favalli[2], Irene Manzella[5], Claudia Romagnoli[6, 4], Francesco Latino Chiocci[3,4], Paul Cole[5], Teresa Nolesini[7], Nicola Casagli[1,8]

[1] National Institute of Oceanography and Applied Geophysics—OGS, Borgo Grotta Gigante 42/C, 34010 Sgonico (Trieste), Italy

[2] Istituto Nazionale di Geofisica e Vulcanologia, Sezione di Pisa, Via Cesare Battisti, 53 - 56125 Pisa, 56125 Pisa, Italy.

[3] Dipartimento di Scienze della Terra, Università degli Studi di Roma "La Sapienza", Piazzale Aldo Moro 5, 00182 Roma, Italy

[4] Istituto di Geologia Ambientale e Geoingegneria, Centro Nazionale Ricerche, UO Sapienza, Piazzale Aldo Moro, 7, 00185 Roma RM

[5] School of Geography, Earth and Environmental Sciences, University of Plymouth, Drake Circus, PL4 8AA Plymouth, UK

[6] Dipartimento Scienze Biologiche, Geologiche e Ambientali, Università degli Studi di Bologna, P.za Porta S. Donato 1, 40126 Bologna, Italy

[7] Centro per la Protezione Civile, Università degli Studi di Firenze, Piazza San Marco 4, 50121 Firenze, Italy

[8] Dipartimento di Scienze della Terra, Università degli Studi di Firenze, Via La Pira 4, 50121 Firenze, Italy

*Corresponding author: Federico Di Traglia (fditraglia@inogs.it)

Abstract

This study analyses the morphological changes induced by eruptive activity at Stromboli volcano (Italy) during and after events occurring during July-August 2019. This period was characterized by intense eruptive activity (two paroxysmal explosions, a two-month-long lava emission, and more intense and frequent "ordinary" explosive activity) that produced significant changes within the region known as Sciara del Fuoco, located on the most unstable, north-western flank of the volcano. Since September 2019, the eruptive activity waned but remained intense, and erosive phenomena continued to contribute to the re-shaping of the Sciara del Fuoco. The morphological changes described here were documented by integrating topographic (PLÉIADES satellite tri-stereo Digital Elevation Models) and multibeam bathymetric data, acquired before, during, and after the paroxysmal events. This allowed the study of the cumulative effect of the different processes and the characterization of the different phases of accumulation/emplacement, erosion, remobilization and re-sedimentation of the volcaniclastic materials.

Data acquired at several periods between September 2018 and April 2020, allowed a comparison of the subaerial and submarine effects of the 2019 events. We find evidence of localized, significant erosion following the two pyroclastic density currents triggered by the paroxysmal explosion of the 3 July 2019. We interpret this erosion as being caused by submarine and subaerial landslides triggered by the propagation of pyroclastic density currents down the Sciara del Fuoco slope. Immediately after the explosion, a lava field accumulated on the sub-aerial slope, produced by effusive activity which lasted about two months. Subsequently, the newly emplaced lava, and in particular its breccia, was eroded, with the transfer of material onto the submarine slope. This work demonstrates how repeated topo-bathymetric surveys allowed identification of the slope processes that were triggered in response to the rapid geomorphological variations due to the eruptive activity. The surveys also allowed distinction of

whether estimated volumetric losses were the result of single mass-flows or gradual erosive processes, with implications on the related geohazard. Furthermore, this work highlights how submarine slope failures can be triggered by the entry into the water of pyroclastic density currents, even of modest size. These results are important for the development and improvement of an early warning system for tsunami-induced by mass flows, both in Stromboli and for island-based and coastal volcanoes elsewhere, where landslides and pyroclastic density currents can trigger significant, potentially destructive, tsunami waves.

Highlights

- 2019-2020 eruption-induced morphological changes at Stromboli were analysed
- data derived from multi-temporal bathymetry and PLÉIADES-1 DEMs
- two paroxysmal explosions, a lava effusion, and intense Strombolian activity occurred
- PDCs generated during the first paroxysmal explosion produced seafloor erosion
- The effusion produced a proximal lava shield and a medial-to-distal debris field

Keywords

Digital Elevation Models, PLÉIADES, Repeated bathymetric surveys, volcano geomorphology, submarine morphology, Stromboli, active volcano, Aeolian Archipelago

1 Introduction

Volcanoes are active geomorphological systems in which morphogenetic processes are induced by dynamic endogenous and exogenous phenomena. Eruptive activity generally leads to the accumulation of material, whereas gravitational processes mainly induce a redistribution of these products (Thouret, 1999; Németh and Martin, 2007).

In this context, volcanic islands and coastal volcanoes are particularly prone to a wide range of hazardous phenomena (Roverato et al., 2020), of which tsunamis are one of the most

significant. During an eruption, tsunamis can be triggered either directly, because of volcanic explosions and the impact of pyroclastic density currents (PDCs) entering the sea (McCoy and Heiken 2000), or indirectly, due to the mass failure along volcanic flanks made less stable by inflation-deflation phenomena, such as dike intrusions (Ward, 2001). Stromboli Island (Figure 1), an active volcano in the Southern Tyrrhenian Sea, is no exception, and since the early 20th century, six significant tsunamis have been recorded which have been generated by mass-flows on its NW flank (1916, 1919, 1930, 1944, 1954, 2002; Maramai et al., 2005; Esposti Ongaro et al., 2021), from the Sciara del Fuoco depression (see Fig 1b; Barberi et al., 1993). The most recent one of these occurred on 30 December 2002 when a 6-7 m wave triggered by submarine-subaerial slope failures of a volume of ~ 20 x 10^6 m^3 , on the NE portion of the Sciara del Fuoco caused extensive damage on the coast of Stromboli (Bonaccorso et al., 2003; Tinti et al., 2005, 2006; Chiocci et al., 2008a, 2008b).

Such dynamic phenomena are strongly related to morphological changes of the volcano. These are key data in determining the stability of the slope, the volumes and velocity of unstable masses that could enter the sea, and the associated hazards. Effective strategies for volcano slope instability detection involves the integration of different methodologies for consistently mapping and monitoring both the subaerial and submarine environments. Such information is typically gathered by field-based studies, geomorphological mapping, remote sensing and geophysical investigations.

The July 2019 - April 2020 eruptive activity at Stromboli is an extraordinary case study for investigating the morphological changes along a steep slope associated with both effusive and explosive phenomena. The activity started on 3 July 2019 with a strong paroxysmal explosion (Giudicepietro et al., 2020; Calvari et al., 2021; Andronico et al., 2021; Giordano and

De Astis, 2021) and continued until the 30 August 2019 with effusive activity (Plank et al., 2020), and another paroxysmal event on 28 August 2019 (Giudicepietro et al., 2020; Turchi et al., 2020; Calvari et al., 2021; Andronico et al., 2021; Giordano and De Astis, 2021). Frequent and intense Strombolian activity and occasional lava overflows from the crater terrace continued until April 2020 (Giudicepietro et al., 2020; Calvari et al., 2021; Aiuppa et al., 2021). This paper analyses the subaerial and submarine morphological variations of the Sciara del Fuoco between September 2018 and April 2020, by using topo-bathymetric data as well as optical images derived from PLÉIADES-1 satellites. Data of the submarine and subaerial parts of the Sciara del Fuoco are available for approximately the same time span, making it possible to assess the geomorphological link between these two sections across several months and multiple significant events. This allows the assessment of mobilized and accumulated volumes associated with different process and help in the understanding of the associated hazards.

2 Materials and Methods

2.1 Study area

The 916 m-high Stromboli Island is the emerged portion of a ~3000 m-high stratovolcano located in the Southern Tyrrhenian Sea off the southern coast of Italy (Figure 1). The volcano has experienced several large mass-wasting phenomena, which formed two large volcano-tectonic depressions, one on its NW flank (Sciara del Fuoco) and the other one on its SE flank (Rina Grande), as a consequence of bilateral flank instability affecting the edifice (Romagnoli et al., 2009). The Sciara del Fuoco depression is filled with volcaniclastic deposits and lavas that are emitted from a summit crater terrace located at ≈ 750 m a.s.l., and from ephemeral vents within the Sciara del Fuoco (Kokelear and Romagnoli, 1995; Casalbore et al., 2010). The distinctive persistent Strombolian activity is characterized by intermittent explosions from the

NE, Central, SW crater areas (NEC, CC and SWC in Fig. 1b) that are located in the summit crater terrace (Rosi et al., 2013). This activity, characterized by intensity and frequency fluctuations over time, is often punctuated by lava overflows from the crater terrace and/or by flank eruptions, with the outpouring of lava flows from ephemeral vents (Di Traglia et al., 2018, 2020).

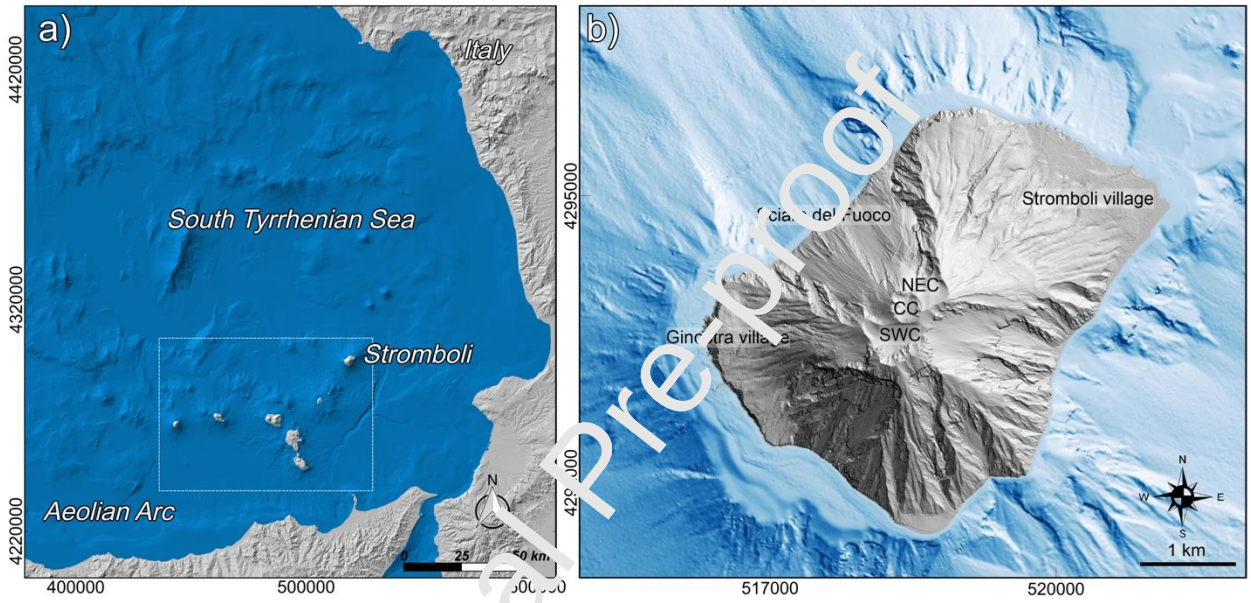

Figure 1. a) Geographic location of the Aeolian Arc in the Southern Tyrrhenian Sea; b) Hill shading-derived DEM of Stromboli Island. Locations of villages, Sciara del Fuoco and main craters (NEC: North East Crater; CC: Central Crater; SWC: South West Crater) are reported.

The Sciara del Fuoco flank is prone to rapid geomorphological changes induced by both volcanic activity and gravitational processes (Chiocci et al., 2008a; Marsella et al., 2012; Bosman et al., 2014; Di Traglia et al., 2018, 2020). Frequent/intense explosive activity and lava effusions produce an accumulation of volcaniclastic deposits mainly on the subaerial slope, whereas periods of less frequent/intense explosions are characterized by erosion of the subaerial Sciara del Fuoco flank and redistribution of the material toward the submarine slopes (Di Traglia

et al., 2018, 2021; Casalbore et al. 2021). Effusive activity produces significant lava accumulations on both the subaerial and submarine slopes, and the initial phases of the effusive flank eruptions are the most critical for the triggering of large landslides (Verrucci et al., 2019; Casalbore et al., 2020).

The 2019-2020 events

On 3 July 2019, Stromboli experienced a paroxysmal explosion (Giudicepietro et al., 2020; Turchi et al., 2020). The explosion generated an eruptive plume around 6-8.4 km in height (Giudicepietro et al., 2020; Giordano and De Astis, 2021; Andronico et al., 2021) and two PDCs that flowed down the Sciara del Fuoco and generated a small tsunami (LGS 2019a). After the July explosion, lava began outpouring from the SWC, and sporadically from the NEC, and this effusive activity , continued until 30 August 2019 (Plank et al., 2019), and intense Strombolian activity continued until April 2020; Calvari et al., 2020). On 28 August 2019, a second paroxysmal explosion occurred (Giudicepietro et al., 2020; Turchi et al., 2020; Giordano and De Astis, 2021), again forming a PDC that moved down the Sciara del Fuoco, generating another small tsunami (LGS 2019b). Subsequently, Strombolian activity remained intense until mid-April 2020, with sporadic overflows from the NEC, and frequent rockfalls and gravel flows linked to the accumulation of erupted material on the edge of the crater terrace (Calvari et al., 2020, 2021).

The chronology of the main events that characterized the volcanic activity at Stromboli between September 2018 and April 2020 are detailed in Plank et al. (2019), and Calvari et al. (2020, 2021) and are summarized in Table 1.

Table 1. *The July 2019 - April 2020 eruptive activity at Stromboli volcano (data from Plank et al., 2019; Calvari et al., 2020, 2021). After the 3 July 2019 paroxysmal explosion, a lava flow from the SWC occurred until 31 August*

2019. During the SWC effusion, Strombolian activity continued, associated with sporadic lava emissions from the NEC and higher intensity explosions (a paroxysm on 28 August 2019 and a major explosion on 29 August 2019). Subsequently, Strombolian activity continued uninterrupted, associated with sporadic effusions from the NEC. ME: Major explosion; PE: Paroxysmal explosion; LF: Lava flow; OF: Overflow.

Date	Type of activity	Description	References
Explosions			
25 June 2019	Type 2 (ME)	Major explosions from CC crater zone	Calvari et al., 2021
3 July 2019	Type 3 (PE)	Explosion from the entire crater terrace. starting from SWC and NEC. Two PDCs along the SdF	Calvari et al., 2021
28 Aug. 2019	Type 3 (PE)	Paroxysm comprising 3 pulses from SWC and NEC. PDC along SdF	Calvari et al., 2021
29 Aug. 2019	Type 2 (ME)	Two fountaining during lava flow	Calvari et al., 2021
Effusions			
3 July 2019 - 30 August 2019	LF	Lava flow from SWC	Plank et al., 2020
12 July 2019	OF	Lava overflow from NEC	This work
18 January 2020	OF	Lava overflow from NEC	This work
5 February 2020	OF	Lava overflow from NEC	This work
28 February 2020	OF	Lava overflow from NEC	Calvari et al., 2020
28 March 2020 - 1 April 2020	OF	Sporadic lava overflows from NEC	Calvari et al., 2020

2.3. PLÉIADES-1 tri-stereo Digital Elevation Models

Topographic change detection of the subaerial part of Sciara del Fuoco was analysed by comparing DEMs generated from PLÉIADES-1 tri-stereo satellite imagery (Bagnardi et al., 2016; Di Traglia et al., 2020). Data used were acquired on 1 September 2018, 13 June 2019, 8 October 2019, and 7 April 2020 (Figures 2, 3 and 4).

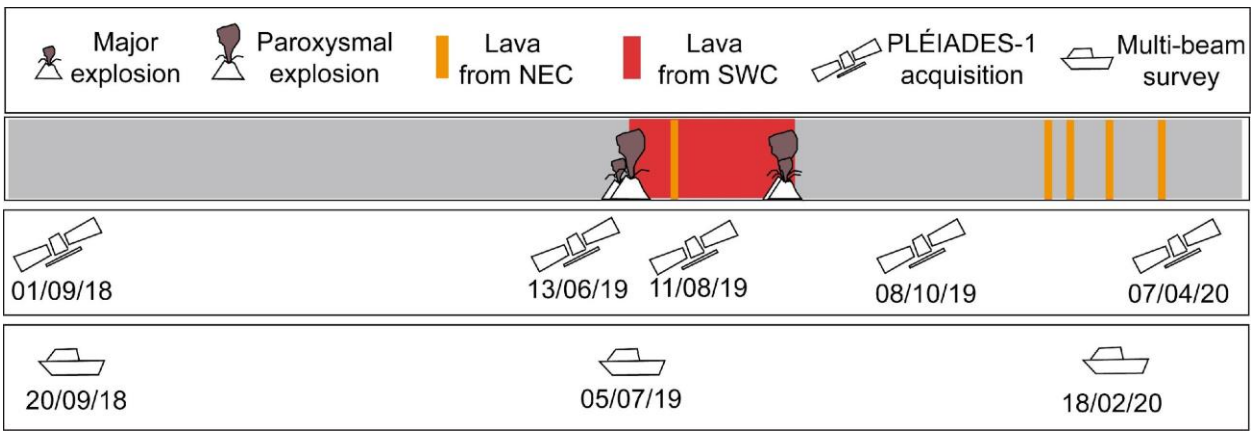

***Figure 2**. Chronology of data acquisitions between September 2018 and April 2020. It also shows the eruptive activity, as reported in Table 1.*

A syn-eruptive PLÉIADES-1 image acquired on 11 August 2019 was used only as an optical image because the disturbance of ash in the atmosphere over the Sciara del Fuoco prevented the generation of a high-quality DEM (Figures 3a and 3b). To assess the accuracy of the heights and their horizontal position in the PLÉIADES-1 DEM, ground control points (GCPs) were collected (cartographic XY standard deviation: 0.15 m). 'Tie points' were automatically collected from the images and the residuals **Δ (X, Y, Z)** estimated for each image (Table 2). As a result a block adjustment including all the satellite scenes was undertaken.

Table 2. Results of the PLÉIADES images adjustment. Mean and root mean square error (RMSE)

Points Residuals (*m*)									
DATE	*13 June 2019*			*8 October 2019*			*7 April 2020*		
	ΔX	**ΔY**	**ΔZ**	**ΔX**	**ΔY**	**ΔZ**	**ΔX**	**ΔY**	**ΔZ**
MEAN	2.1595	0.0582	0.501	3.9519	0.0622	2.802	0.1600	0.0940	-0.180
RMSE	3.2791	1.0054	0.841	4.0242	1.0373	3.565	0.3336	0.2844	1.320

2.4. Multibeam acquisitions

Three bathymetric surveys off the Sciara del Fuoco were carried out between 2018 and 2020 at water depths of 2-400 m in the framework of the periodic monitoring of the Sciara del Fuoco, which began in 2002, after the 2002-03 eruptive crisis (Chiocci et al., 2008a, 2008b). The first bathymetric survey was realized between 5 and 400 m water depth on 20 September 2018 by IDROSFERA onboard the small vessel "2NA1932" through the multibeam echosounder "R2Sonic" operating at a frequency of 200 kHz. The multibeam system emitted 256 beams, each of them characterized by a beam width of 0.5°x1° (across and along-track, respectively). Data

were positioned through RTK LEICA Serie 1200 and DGPS Hemispher V103. The bathymetric data were acquired and processed with Qinsy QPSTM ver. 8.18.3. Processed data were gridded with a cell-size of 2 m.

The second bathymetric survey was realized on 5 July 2019 (two days after the 3 July 2019 paroxysm) between 5 and 400 m water depth by the "Istituto Idrografico della Marina" onboard the Research Vessel "Magnaghi" and the small vessel "MBN 118" using the multibeam systems Kongsberg EM2040 ed EM2040C 8 working at a frequency of 200 kHz. Data were positioned through DGPS FUGRO 9205 e SPS855, with differential corrections obtained by means of the Marinestar HP/XP G2. Data were processed with Caris Hips and Sips using the CUBE algorithm and gridded with a cell-size of 2 m. However, soundings are characterized by high level of stochastic and systematic noise (especially for the outer beams) due to bad weather conditions (i.e., rough sea) occurring during the survey. This noise was partially filtered during the processing, but some parts of the DEM are still characterized by a high level of noise, making the interpretation of specific features problematic, and affecting reliable volumetric computation in such areas as highlighted in section 2.5.

The third bathymetric survey was realized between 1 and 400 m water depth on 18 February 2020 by Arena Sub onboard the small vessel "Valerio" using the multibeam system Reson 7125 working at a frequency of 200 kHz. Data were positioned through Trimble Applanix Pos Mv and processed with PDS2000 software. Data were gridded with a cell-size of 2 m.

Tidal corrections for all the multibeam surveys were applied using tide gauge data recorded at Stromboli by I.S.P.R.A (www.mareografico.it).

2.5. DEM co-Registration, error estimation, and Topographic Change Detection

Topographic change detection (TCD) using multi-temporal DEMs was performed by differencing two DEMs of the same area derived from data acquired at different times. This

calculation is typically affected by errors associated with mismatches between two DEMs of the same area, which leads to artefacts in elevation differences (Δh) (Favalli et al., 2010). Such errors can be detected and quantified, and possibly reduced by measuring and minimizing the DEM differences in areas of the two DEMs considered to be equal, i.e., those areas that are not affected by relevant changes.

In this work, PLÉIADES DEM-to-DEM co-registration was based on the minimization of the root mean square (RMS) error between one DEM and another by iteratively varying the three angles of rotation, the translation, and the magnification or reduction factor of one DEM by using a custom-made algorithm based on the MINUIT minimization library (e.g. Favalli et al., 2018). MINUIT is a tool that can be used to find the minimum value of multiparameter functions (http://www.cern.ch/minuit). We followed the same workflow described in Di Traglia et al. (2020) for the co-registration of PLÉIADES DEMs, which mainly consists of the registration of one DEM using a second as ground truth and by taking a given number of areas without relevant natural changes around the region of interest as matching areas. After the two DEMs are co-registered, they are compared and the RMS displacement error ($\sigma_{\Delta Z}$) calculated over areas without significant change.

In this work, the following DEM differences were calculated: i) June 2019 - September 2018 DEMs; ii) October 2019 - June 2019 DEMs; iii) April 2020 - October 2019 DEMs; and iv) April 2020 - September 2018 DEMs, which covered the whole period of data acquisitions (Figure 4). The $\sigma_{\Delta Z}$ were, respectively, 0.56 m, 0.61 m, 0.54 m and 0.61 m.

The bathymetric data were treated with the same method, but the displacement error was still significant after the co-registration procedure and so no corrections were applied. The following bathymetric differences were calculated: i) July 2019 - September 2018; ii) February

2020 - July 2019; and iii) February 2020 - September 2018, which covered the whole period of data acquisitions (Figure 5). The $\sigma_{\Delta Z}$ were, respectively, 3.12 m, 2.63 m and 1.84 m.

The differences between two successive co-registered DEMs were used to detect and outline the extent of areas that were affected by topographic changes (Figures 4 and 5) and to calculate the volume and thickness variation inside them (Table 3). Moreover, the geomorphological mapping of the Sciara del Fuoco was conducted through the analysis of the orthorectified PLÉIADES-1 images. The volume (*V*) emplaced or lost between two acquisitions was calculated from the DEM difference according to the equation: $V = \sum_i \quad \Delta x^2 \Delta z_i$ (Favalli et al., 2010), where Δx is the grid step and Δz_i is the height variation within the grid cell *i*. These values were then summed for all the cells in the selected areas in which the volume changes were calculated. An upper bound on the error for the volume estimate was given by assigning to each pixel the maximum possible error, i.e., $Err_{V,high} = A\sigma_{\Delta Z}$, where *A* is the investigated area (Favalli et al., 2010).

3 Results

Based on the results of the analysis of the PLÉIADES-1 imagery, the morphology of the 2019 lava flow field was characterized (Figure 3). Detection of topographic changes were estimated only in the Sciara del Fuoco area (Figure 4 and Table 3), as a result of the crater terrace covered by the gas plume in all the PLÉIADES-1 images. The 8 October 2019 – 13 June 2019 difference map (Figure 4b) allowed the estimation of the total volume emplaced on the subaerial slope, comprising the lava-and-debris field (S1A; $2.130 \pm 0.157 \times 10^6$ m^3), and a lava overflow emitted from the NE craters (S3A; $0.022 \pm 0.004 \times 10^6$ m^3). Localized accumulation and erosion zones have been identified (S2A and S1E).

The last pair of DEMs (comparison 20 April 2020 – 8 October 2019, Figure 4c) allowed

estimation of both the continuous accumulation of material in the proximal areas, in the talus beneath the NE craters (S5A; 0.070 ± 0.013 × 10^6 m^3), and the volume of the overflow emitted by the NE craters on late March 2020 (S5A; 0.157 ± 0.031 × 10^6 m^3, in agreement with previous estimation of Calvari et al., 2020). The 20 April 2020 – 8 October 2019 comparison (Figure 4c) shows that marked erosion has occurred in the 2019 volcaniclastic deposits at the foot of the Sciara del Fuoco slope (S3E; -0.555 ± 0.031 × 10^6 m^3; S4E; -0.385 ± 0.044 × 10^6 m^3). In Figure 4d it is possible to note the morphological variations in the subaerial Sciara del Fuoco, in which it is possible to note the accumulation and erosion zones that were generated during the whole investigated period.

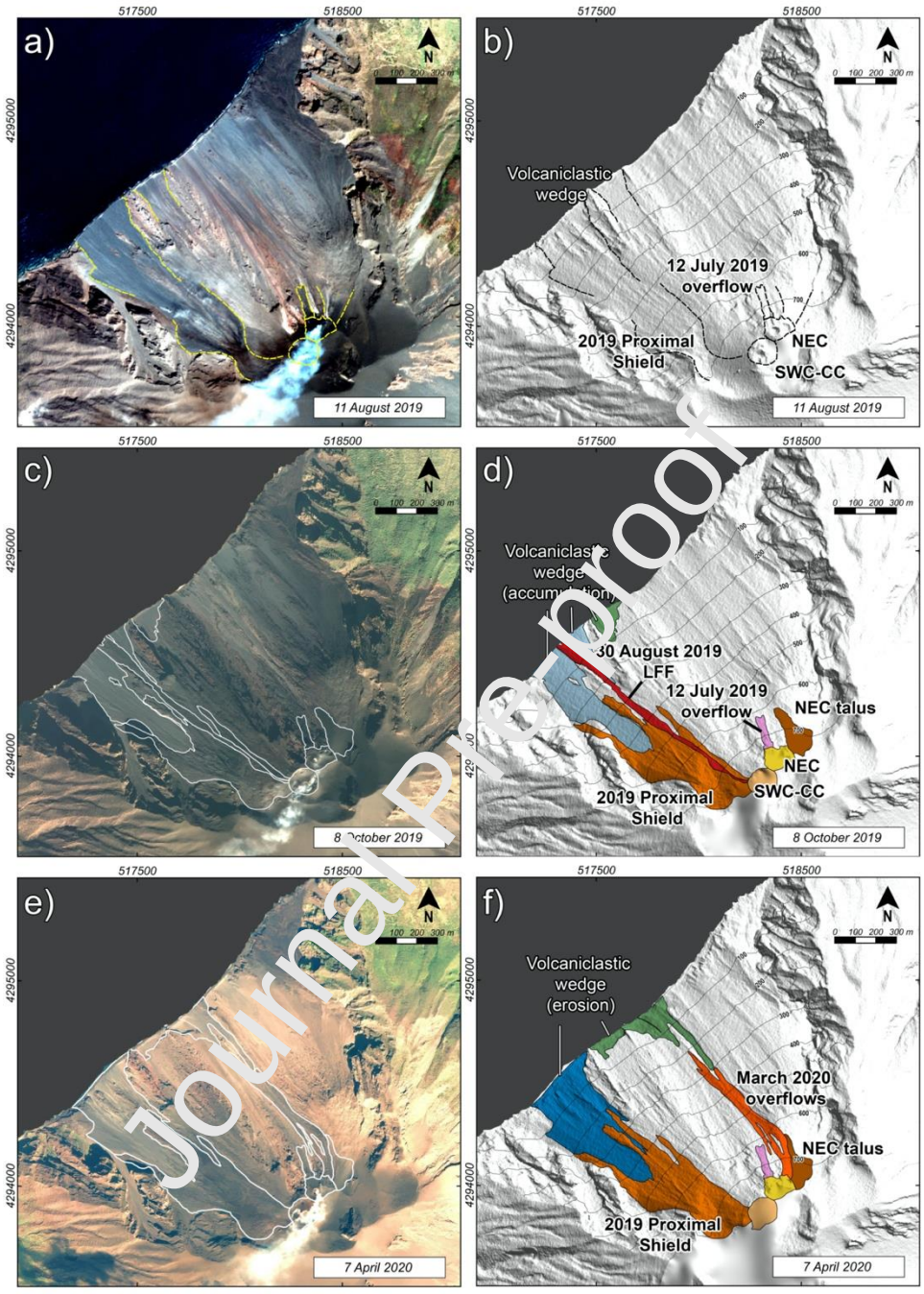

Figure 3. Geomorphological mapping of the subaerial part of the Sciara del Fuoco, based on PLÉIADES-1 optical images and tri-stereo DEMs. In a) and b) the details on the Sciara del Fuoco area during the 2019 eruption (11 August 2019) are evidenced, where it is possible to highlight the initial stages of the 2019 lava flow field (LFF), with the formation of the proximal shield and the volcaniclastic wedge; in c) and d) the Sciara del Fuoco area on 8 October 2019, where the complete development of the 2019 lava flow field is evident; in e) and f) data collected on 7

April 2020 evidenced the erosion of the volcaniclastic wedge, as well as the development of the NEC talus and the placement of overflows during March 2020. See text for details. (LFF: Lava Flow Field; NEC: North East Crater; CC: Central Crater; SWC: South East Crater. The geomorphological interpretation of the processes is mainly based on the textural differences of the PLÉIADES-1 optical images. The estimated accumulated/removed volumes are shown in Figure 4.

Table 3. Topo-bathymetric change detection results (see Figures 4, 5 and 6 for zones location). $\sigma_{\Delta Z}$ of sectors T1A and T1E are calculated combining the $\sigma_{\Delta Z}$ of the April 2020 - September 2018 DEMs difference and the the $\sigma_{\Delta Z}$ of April 2020 - September 2018 bathymetric difference, taking into account the corresponding areas (Figure 6). *In some cases, the error in the thickness estimate is greater than the thickness itself. This is due to the noise of the data, especially in the survey of 5 July 2019.*

	Zone	Description	Area ($\times 10^6$ m^2)	Volume ($\times 10^6$ m^3)	Mean Thickness (m)	$\sigma_{\Delta Z}$ (m)
ACCUMULATION	S1A	2019 Proximal shield	257.50	2.130 ± 0.157	8.3	0.61
	S2A	Volcaniclastic wedge	14.24	0.042 ± 0.009	3.0	0.61
	S3A	12 July 2019 overflow	6.13	0.022 ± 0.004	3.6	0.61
	S4A	NEC-Talus	20.47	0.070 ± 0.013	3.4	0.61
	S5A	NEC-Talus and March 2020 overflows	56.33	0.157 ± 0.031	2.8	0.54
	M1A	Submarine accumulation	44.33	0.212 ± 0.117	4.8	2.63
	M2A	Submarine accumulation	16.42	0.067 ± 0.043	4.1	2.63
	M3A	Submarine accumulation	63.72	0.220 ± 0.167	3.5	2.63
	M4A	Submarine accumulation	13.78	0.037 ± 0.036	2.7	2.63
	T1A	Subaerial-submarine accumulation	98.36	0.250 ± 0.154	2.5	1.57
EROSION	S1E	Subaerial erosion	44.85	-0.111 ± 0.027	-2.5	0.61
	S2E	Subaerial erosion	7.81	-0.027 ± 0.009	-3.4	0.61
	S3E	Subaerial erosion	57.62	-0.555 ± 0.031	-9.6	0.54
	S4E	Subaerial erosion	81.39	-0.385 ± 0.044	-4.7	0.54
	M1E	Submarine landslide/erosion	51.35	-0.176 ± 0.160	-3.4	3.12
	M2E	Submarine landslide/erosion	208.63	-1.119 ± 0.652	-5.4	3.12
	M3E	Submarine erosion	32.45	-0.080 ± 0.085	-2.4	2.63
	M4E	Submarine erosion	26.38	-0.071 ± 0.069	-2.7	2.63
	M5E	Submarine erosion	23.07	-0.042 ± 0.061	-1.8	2.63
	T1E	Subaerial-submarine erosion	386.72	-1.551 ± 0.587	-4.0	1.51

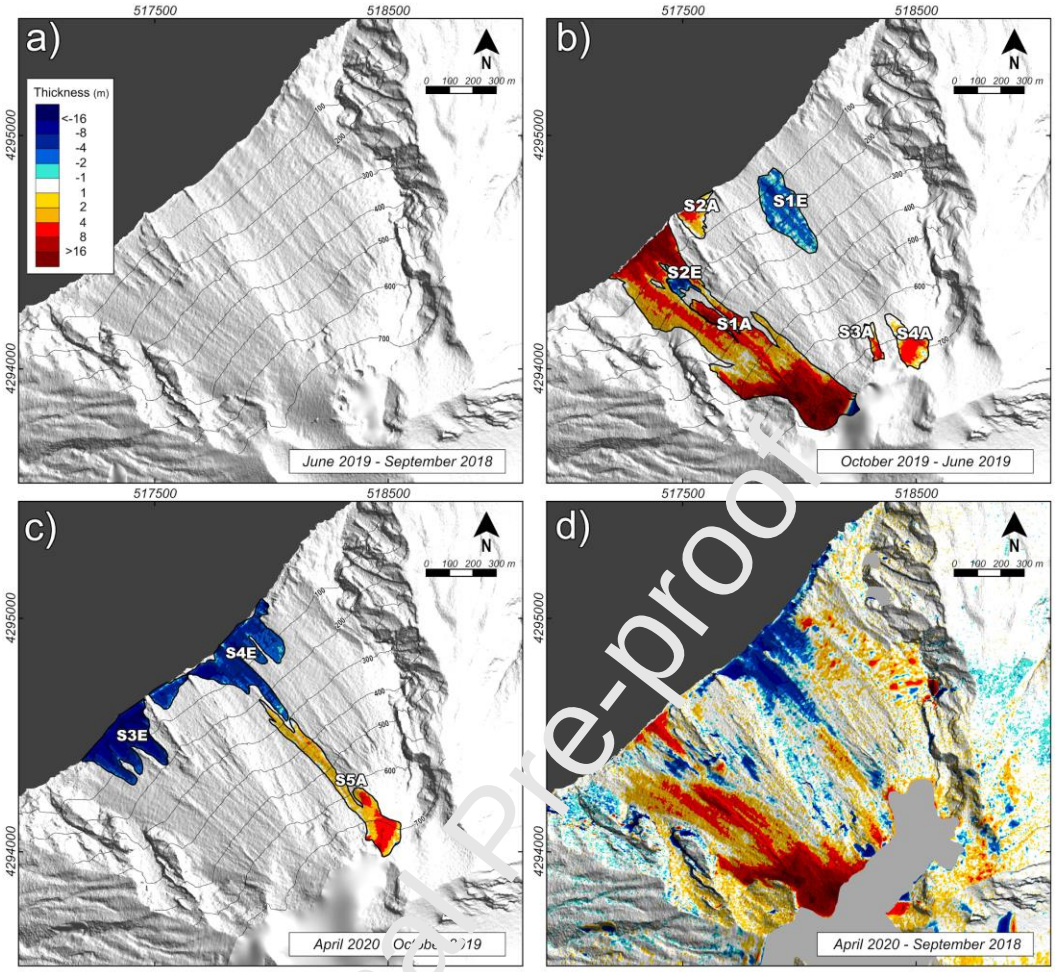

Figure 4. Sciara del Fuoco topographic change detections between September 2018 and April 2020 through PLÉIADES DEMs comparison. The legend is the same for all frames. a) June 2019 vs. September 2018. No morphological changes are detectable at the scale of observation; b) October 2019 vs. June 2019. The main morphological changes are due the 3 July 2019 and 28 August 2019 explosions; c) April 2020 vs. October 2019. The main morphological changes are related to the erosion of the lowest sector of the SdF and to March 2020 overflow; d) April 2020 vs. September 2018 comparison shows the morphological changes of the aerial sector of the SdF in the whole time of investigations. The frames a), b) and c) were cleaned for the residual mismatching between DEMs after the coregistration. Frame d) was not cleaned to show the distribution and the magnitude of the residual mismatching between DEMs.

The survey undertaken two days after the 3 July 2019 paroxysm, enabled a detailed

characterisation of the seafloor changes associated with this event, as well as the following morphological evolution of the submarine part of the Sciara del Fuoco.

The difference map obtained between the pre- and post-3 July 2019 paroxysm shows that the morphological changes are largely dominated by submarine erosion, mainly located in the SW (M1E in Figure 5a) and central (M2E in Figure 5a) zones. The M1E, occured in an area that had never been affected by erosion/landslides since the periodic bathymetric monitoring of the Sciara del Fuoco began in 2002 (Chiocci et al., 2008b; Casalbore et al., 2020 and 2021), and was characterized by a negative difference between the bathymetry of 29 September 2018 and that of 5 July 2019. It involves an area of 51.35 x 10^3 m^2, with a mean removed thickness of 3.4±3.12 m, equal to an eroded/collapsed volume of 0.176 ± 0.160 x 10^6 m^3 (Table 3; note that the large error is due to the noise of the data in the survey of 5 July 2019). The area affected by seafloor erosion in the central part of the Sciara del Fuoco (Figure 5a, M2E), affected 208.63 x 10^3 m^2 of the seafloor, with a mean removed thickness of 5.4±3.12 m, and an estimated volume of 1.119 ± 0.652 × 10^6 m^3 (Table 3). The maximum eroded thickness (~20 m) is observed between the coastward limit of the 5 July 2019 survey in this sector (i.e., 15 m water depth) and the 110 m water depth, outlining the shape of a possible landslide scar. The volume of this landslide scar is underestimated because its thickness is still relevant (~10 m) at the water depth of 15 m (limit of the 2019 survey), indicating that the landslide scar continued coastward, into the subaerial region. Moreover, the 2019 morpho-bathymetry shows an uneven setting of this area, with the coalescence and superimposition of multiple small-scale landslide scars and fan-shaped deposits, suggesting a complex morphological evolution of the seafloor directly associated with the 3 July 2019 paroxysm. A minor amount of accumulation was also detected in shallow water on the SW SdF slope (see area in yellow outside the field of T1A in Fig. 6); however, its volume has not

been estimated considering the errors associated with the comparison between July 2019 and September 2018 DEMs.

The comparison between the 18 February 2020 and 5 July 2019 bathymetries shows, instead, a general seafloor accretion (Figure 5b). It should be noted that the error in the volume calculation, in some cases, is again particularly high (up to 100%) due to the noise of the data in the survey of 5 July 2019, and as such the analysis should be tentative. The SW portion of the Sciara del Fuoco shows an overall accretion (M1A+M2A) down to 350 m water depth over an area of ~0.35 x 10^6 m^2 accounting for an estimated volume of ~0.7 x 10^6 m^3. The largest thicknesses (up to 9 m) are observed in the 20-120 m depth range, rapidly decreasing in both downslope and upslope directions (Figure 5b).

In the 18 February 2020 - 5 July 2019 comparison, in the central area of the Sciara del Fuoco major changes occurred (Figure 5a). Here, the submarine slope is characterized by a patchy distribution of seafloor accretion and erosion, mainly affecting the large depression identified in the 2019-2018 difference map (Figure 5a). The area that was affected by the maximum removal of material between 2019 and 2018 DEMs (zone M2E in Figure 5a) was subsequently the location of both accumulation phenomena (M3A and M4A, in Figure 5b) and further erosion (M3E and M4E in Figure 5b). The added volume is $0.220 \pm 0.167 \times 10^6$ m^3 and $0.037 \pm 0.036 \times 10^6$ m^3 for areas M3A and M4A, respectively. Seafloor erosion reached volumes of $-0.080 \pm 0.085 \times 10^6$ m^3 and $-0.071 \pm 0.069 \times 10^6$ m^3 for areas M3E and M4E, respectively. Outside the main erosion/landslide depression of the central Sciara del Fuoco, another eroded area was identified to the East, equal to a volume of $-0.042 \pm 0.061 \times 10^6$ m^3 (zone M5E in Figure 5b).

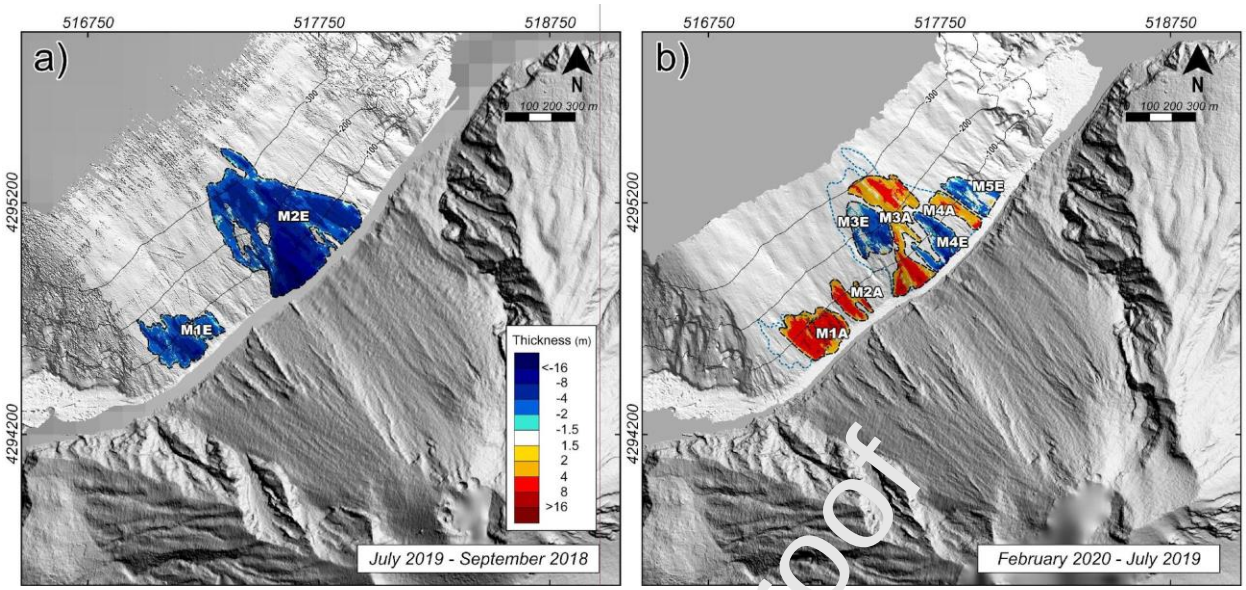

Figure 5. Sciara del Fuoco bathymetric change detections: a) July 2019 - September 2018; isobaths every 100 m (derived from the 2019 bathymetry). b) February 2020 - July 2019; isobaths every 100 m (derived from the 2020 bathymetry).

The 2020-2018 merged topo-bathymetric difference map (Figure 6) and profiles (see the Supplementary Materials to this article for profiles location and tracks) reveals that the SW and central part of the slope are the two areas affected by the main morphological changes across the overall monitoring period, but with different evolutions that are hereafter compared between the subaerial and submarine slope. In the SW sector, the subaerial slope evolved with the initial emplacement of the 2019 lava-and-debris field, which was subsequently eroded (April 2020 - October 2019 DEMs difference; Figure 4c), leaving only the proximal shield as well as a small part in the coastal area. In the submarine slope, after an initial erosion surpassing deposition (as derived from the 2019-2018 difference, Figure 5a), the accumulation of material prevails, with the development of a series of coalescing and smooth fan-shaped morphologies (T1A in Figure 6), likely due to the erosion of the subaerial debris field emplaced during effusive activity in 2019. Additional accretion in the submarine sector is observed at greater depths (down to 350

m), showing an overall patchy distribution. In the central Sciara del Fuoco erosion prevails (T1E in Figure 6), affecting the volcaniclastic deposits at the foot of the subaerial slope (see topographic change detection in April 2020 - October 2019 DEMs difference, Figure 4c) and, particularly, the submarine slope after the 3 July 2019 paroxysm (Figure 5a and section P3 in Supplementary Material). In the latter area, erosion is not compensated by subsequent accumulation phenomena observed in the 2020 survey (Figure 5b).

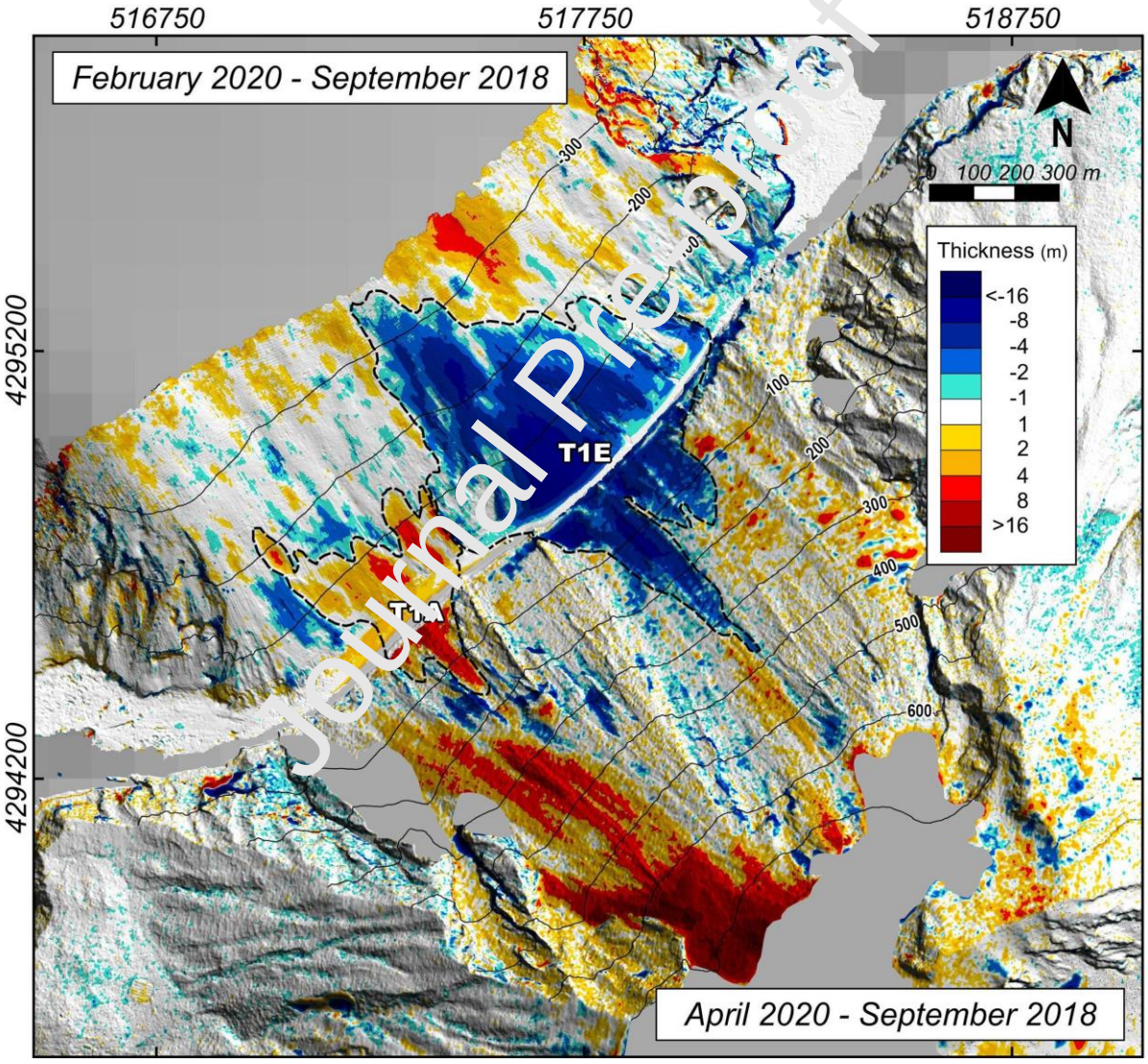

Figure 6. 2020 - 2018 subaerial-submarine morphological changes. The subaerial part is derived from the April 2020 - September 2018 PLEIADES DEM comparison, the submarine part from the February 2020 - September 2018 bathymetry (isobaths every 100 m are derived from the February 2020 bathymetry; contour lines every 100 m are

derived from the April 2020 DEM). Topo-bathymetric profiles are included in the Supplementary Materials to this article.

4 Discussion

The availability of both bathymetric and topographic data, acquired in close time windows, has allowed a comprehensive analysis of the geomorphological changes across the Sciara del Fuoco over two years of observations between 2018 and 2020. This period is characterized by the occurrence of significant eruptive events, with both effusive and explosive phenomena, and by non-eruptive periods. Analysis of the accumulation-erosion-remobilization phenomena in the Sciara del Fuoco subaerial and submarine slope is presented in terms of slope morphological response to different dynamics (Figure 7).

The 2019 lava flow field is the first to be emplaced in the SW sector of the Sciara del Fuoco since the 1967 eruption (Marsella et al., 2012). Some features are typical of other Stromboli lava flow field morphologies produced by a high-elevation vent, as described for the 2002–2003 lava flow field (Lodato et al. 2007) and that of 2014 (Casalbore et al. 2021). These features are: i) a proximal shield, formed beneath the SWC area (Fig 3d); and ii) a volcaniclastic wedge emplaced from ~ 470 m a.s.l. to the shoreline (Figure 3d). The main difference between the 2019 field and, at least for the last four lava flow fields (i.e., 1985, 2002-03, 2007 and 2014) is the absence of an intermediate zone fed by small lava flows in the subaerial part. Another marked difference is the lack of well-defined morphological ridges in the submarine slope linked with marked seafloor accretion which were observed in 2007 and 2014 eruptions at Stromboli, being related to a more coherent lava flow (Bosman et al., 2014; Casalbore et al., 2021). Similar features were seen at the larger effusive eruption which occurred in 2018 at Kīlauea volcano, Hawaii (Soule et al., 2021). This evidence supports the fact that seafloor accretion during the 2019-2020 effusive

activity was mainly made up of lava breccias likely due to the low effusion rates and vent location. It is noteworthy that lava breccias dominated the architecture of an ancient submarine ‘a’ā lava-fed delta in Antarctica, forming together with coherent submarine emplaced lavas in a chaotic arrangement collectively termed “lobe hyaloclastite” (Smellie et al., 2013).

During the analysed period, the positive values obtained from the elevation differences between DEMs in the subaerial slope (Figure 3 and 4; Table 3) are considered due to: the emplacement of the 2019 lava field, comprising an overflow that began on the 12 July 2019 and multiple overflows that occurred during late March 2020, and the accumulation of volcaniclastic material under the NE crater, and along the coastline. The accumulations calculated in this work should also be added to the deposits of the crater area, which have been estimated by Civico et al. (2021) to a total of ≈0.5 x 10^6 m^3 between September 2018 and June 2020. Conversely, the negative values observed in the subaerial slope (Figure 3 and 4; Table 3) are related to the erosion of the 2019 lava field and of the volcaniclastic wedge along the coastline.

The main erosion observed in the Sciara del Fuoco started in its submarine sector and evolved later into the subaerial part (T1E in Figure 6), likely due to retrogressive erosion. The accumulations in the submarine area, on the other hand, are due to the erosion of the subaerial slope and occur after the end of the eruption. In fact, the maps in Figures 4 and Figure 5 show that a large part of the submarine accumulation is due to the erosion, transport and redeposition of the material that formed in the subaerial part during the 2019 events, indicating a rapid transfer of material once the eruptive activity waned. While the occurrence of accumulation areas and their migration over time can be readily explained by the emplacement of the 2019 lava field and volcaniclastic wedge (Figure 7b), as well as by their subsequent erosion and remobilization from the subaerial to the submarine slope (Figure 7c), it is more difficult to explain the presence

of the two main erosion areas in the difference map between the 2018 and 2019 surveys (Figure 7a). Since 2002, the periodic bathymetric monitoring of the Sciara del Fuoco has recorded appreciable submarine erosion only associated with the 30 December 2002 tsunamigenic landslide linked to small-scale slope instability induced by major storms (Chiocci et al., 2008a,b). The size of the depression M2E (Figure 5a) is comparable in size with the erosion observed just below the entrance point of the 2014 lava flows (Casalbore et al., 2021) and markedly smaller than that of the landslide scar of the 30 December 2002 (about 10% in volume) It is, however, much greater than that due to erosion typically linked to storm activity on the shallow submarine slope (see Chiocci et al., 2008b). Observations made during the explosion (Giordano and De Astis, 2020) showed that both the PDCs generated by the paroxysmal explosion of 3 July 2019 entered the sea exactly in the location of the M1E and M2E erosional areas we observe in the bathymetry (Figure 5a). It is unclear whether subaerial PDCs, such as those observed in these events, can trigger submarine instability in the Sciara del Fuoco, although analogue models suggest that mass-flow induced overload is capable of generating retrogressive landslides (Nolesini et al., 2013), consistent with that observed in the topo-bathymetric data. The erosive potential of PDCs entering the sea has been suggested offshore Montserrat during the 1996-1998 eruptions of the Soufrière Hills volcano, where the entry points of some PDCs match erosive areas reconstructed in the proximal part of the submarine flank through bathymetric comparison (Hart et al., 2004). During the same period PDCs were observed to be highly erosive on land, with extensive removal of vegetation and topsoil (Cole et al. 1998).

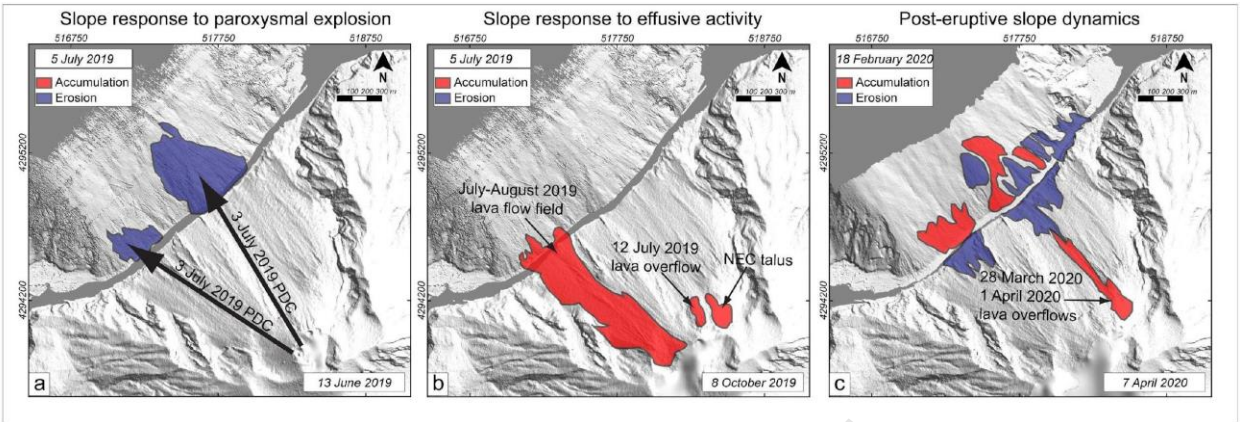

Figure 7. Schematic representation of the evolution of the Sciara del Fuoco slope.

Using the multi-temporal approach proposed here, it is thus possible to define the main geomorphological processes that influence the different parts of the Sciara del Fuoco as a function of the observed phenomena during syn-eruptive and post-eruptive stages.

In summary, the accumulation-erosion phases that the slope of the Sciara del Fuoco has undergone can be summarized as follows:

a) a strong paroxysmal explosion that took place on 3 July 2019 generated two PDCs that induced mostly landslide/erosion in the upper submarine slope;

b) effusive activity that took place between 3 July 2019 and 31 August 2019 generated a lava field that developed mainly on the sub-aerial slope, and to a lesser extent on the submarine one;

c) the end of the intense eruptive activity coincided with the start of the reworking of the subaerial slope, both with the erosion of the volcaniclastic wedge, and as the retrogressive evolution of the landslide/erosion depression that was generated in the central part of the submarine Sciara del Fuoco slope. This subaerial erosional activity has remobilized material, partially filling the submarine depressions, even if the final geometry derived from the long-term difference (2018-2020) identifies a single, main

depression with perfect continuity between the submarine and subaerial slopes (T1E).

In general, the proximal area (around the crater terrace) is characterized by accumulation and erosion (crater-rim slides, vertical collapses and craterization), which depend on the style and intensity of the eruptive activity. While the Sciara del Fuoco slope experienced mainly subaerial accumulation processes during the high-intensity (frequent explosions and effusions) eruptive activity, the volcaniclastic apron located between the coastline and 300-400 b.s.l. (see Chiocci et al., 2008a and Casalbore et al., 2010) received material from upslope mostly when the intense eruptive activity waned, and erosive processes mainly influenced the dynamics of the subaerial slope. The erosion of material at Stromboli occurs with small rockfalls and debris slides, which evolve into gravel flows along the Sciara del Fuoco. This increases the landslide hazard in the first tens, and in some cases hundreds, of meters from the coastline. This conceptual scheme is effective for effusive activity with vents located at high altitudes (650-750 m a.s.l.), while for effusive eruptions characterized by vents located at low altitudes (e.g. eruption 2007; Bosman et al., 2014), the submarine part is directly fed by the eruptive activity, building lava deltas at the coast and potentially increasing the submarine slope instability.

Making a comparison with similar cases is not easy, considering that data of such high accuracy and temporal frequency are nearly unique, especially in active volcanic areas. Similar volcanoes to Stromboli, in terms of activity, style and morphology, include Batu Tara in Indonesia (Laiolo et al., 2018; Spina et al., 2021). However, there are no topo-bathymetric data that allow to reconstruct a geomorphological evolution of the volcano that can be compared with those of Stromboli.

Moreover, from the analyses presented here, it is not clear whether the eroded areas detected following the paroxysmal explosion of 3 July 2019 were produced by landslides triggered by PDCs, or if instead these are the product of particle entrainment by PDCs on the seafloor, and

therefore of bulking of PDCs. themselves. However, this study demonstrates that there is a need to consider these phenomena in the modelling of tsunamis induced by PDCs. While the possibility of triggering submarine landslides caused by overloading has been taken into consideration (e.g. Nolesini et al., 2013; Casalbore et al., 2020), and refers to the well-known trigger mechanism of landslides for an undrained load (e.g. Sassa and hui Wang, 2005), this cascade trigger has not been considered previously in tsunami modelling.

As for PDCs-induced tsunami modelling considering flow bulking, particle entrainment is studied in PDC motion, deposit and runout, and the effects of temperature as well (e.g. Roche, 2015; Fauria et al., 2016; Pollok et al., 2016; Shimizu et al., 2019). Unfortunately, there are currently no numerical models that consider the effect of PDC bulking during tsunami triggering (e.g. Maeno and Imamura, 2007). Therefore, this study can be considered as the starting point to develop and validate models of tsunami triggering by mass-flows, in order to consider both the cascade triggering effects (tsunamis induced by PDC + landslides), and the effect of PDC bulking in triggering tsunamis.

5 Conclusions

This study analyses the morphological variations in the Sciara del Fuoco depression induced by the 2019 eruption of the Stromboli volcano, as well as in the period following the eruption. This was possible thanks the collection of bathymetric and topographic data at comparable time intervals, before, during, and after the 2019 events. Our analysis shows that a multi-temporal approach with frequent surveys in a highly dynamic environment, at such an active volcano, is the only way to estimate the emitted/remobilized volumes with a significant level of detail.

The 2019 events were characterized by intense explosive activity (two paroxysmal explosions,

more intense and frequent "ordinary" explosive activity), as well as by the emplacement of a lava-and-debris field in the SW part of the Sciara del Fuoco depression. This began with a sudden, paroxysmal explosion that occurred on 3 July 2019 and generated two PDCs that flowed down the volcano's flanks, which triggered a 1.5 m tsunami less than 1 km from the Sciara del Fuoco. In correspondence with the entry points of the two PDCs into the water, two depressed areas formed in the seafloor; a larger one in the centre and a smaller one in the SW part of Sciara del Fuoco. Their geometry is compatible with the occurrence of submarine and subaerial landslide scars. We tentatively suggest a cause-effect relationship between the entry into the water of the PDCs and the triggering of submarine instability phenomena in the Sciara del Fuoco slope. The effusive activity produced a lava field consisting of a proximal shield and a debris field placed on the subaerial slope. The 2019 lava flow field lack of well-defined morphological ridges in the submarine slope linked with marked seafloor accretion which were observed during previous eruptions Stromboli, as well as in 2018 at Kīlauea volcano. The 2019 debris field was heavily eroded after the end of the eruption, causing accretion of the seafloor. During the period following the main eruption, the eruptive activity remained intense, but exogenous phenomena also contributed to the re-shaping of the Sciara del Fuoco.

Topographic and bathymetric data acquired with high acquisition frequency are rare. Furthermore, bathymetric data acquired close to the coast of an active volcano with persistent activity are even more rare. These conditions make comparison with other natural cases difficult. For example, during the recent activity of the Soufriere Hills in Montserrat (1995 - 2010) many topographical and bathymetric studies were carried out, however: 1) they were conducted separately, and 2) bathymetric surveys were not made close to the coast, for obvious hazard reasons.

To conclude, it is possible to state that Stromboli is an exceptional case study for analysing the geomorphological response of a volcano's flank in a highly dynamic environment. The persistent Strombolian explosions of different intensity and frequency, punctuated by effusive activity, constantly produce considerable quantities volcaniclastic debris at the summit craters, and sporadically form vents within the Sciara del Fuoco. The volcano's steep slopes induce the continuous re-mobilization of the volcaniclastic material, through instability phenomena at different scales. Effusive eruptions with high-elevation vents (> 550 m a.s.l.) will favour the growth of the subaerial slope, generally being more stable, and which is rebalanced by erosive phenomena. On the contrary, low-elevation vents fed lava flows that may accumulate considerable (even > 10^6 m^6) debris (lavas and breccias) in the underwater slope, increasing the load and the predisposition of accumulated material to collapse through landslides (>10^6 m^3).

While large landslides (>10^7 m^3) have been observed mostly in response to magmatic intrusions in the Sciara del Fuoco, instability phenomena of considerable size (~ 10^6 m^3) can be caused by explosive eruptions, and the consequent load of the seabed by the emplacement of PDCs. However, the evidence of the 2019 eruption shows that small PDCs (<10^6 m^3), in addition to triggering small tsunamis, induce seabed erosion / landslides. Studies on the potential of triggering of tsunamigenic landslides induced by larger PDCs are necessary. This result is particularly important in the development and improvement of tsunami early warning systems, where all the factors causing mass flows, and possibly significant waves, need to be considered as potentially destructive and dangerous phenomena.

Acknowledgments

Funding: This research was funded by the "Presidenza del Consiglio dei Ministri–Dipartimento della Protezione Civile" (Presidency of the Council of Ministers–Department of

Civil Protection), through the UniFi-DPC 2019-2021 agreement (Scientific Responsibility: N.C.) and the CNR-IGAG – DPC agreement 2019-2022 (Scientific responsibility: F.L.C). The contents of this paper represent the authors' ideas and do not necessarily correspond to the official opinion and policies of the "Presidenza del Consiglio dei Ministri–Dipartimento della Protezione Civile" (Presidency of the Council of Ministers–Department of Civil Protection).

This research was also funded by the NERC Project "Tsunamigenic mass flows at Stromboli Volcano- analysis and modelling after the 3rd of July events" (NE/T009438/1; Scientific Responsibility: I.M.).

The authors are grateful to the editor for managing the publication, to the reviewers for the comments that have improved the manuscript.

References

Aiuppa, A., Bitetto, M., Delle Donne, D., La Monica, F. P., Tamburello, G., Coppola, D., Della Schiava, M., Innocenti, L., Lacanna, G., Laiolo, M., Massimetti, F., Pistolesi, M., Silengo, M. C., Ripepe, M. (2021). Volcanic CO2 tracks the incubation period of basaltic paroxysms. Science Advances, 7(38).

Andronico, D., Del Bello, E., D'Oriano, C., Landi, P., Pardini, F., Scarlato, P., de' Michieli Vitturi, M., Taddeucci, J., Cristaldi, A., Ciancitto, F., Pennacchi, F., Ricci, T., Valentini, F. (2021). Uncovering the eruptive patterns of the 2019 double paroxysm eruption crisis of Stromboli volcano. Nature Communications, 12(1), 1-14.

Bagnardi, M., González, P. J., & Hooper, A. (2016). High- resolution digital elevation model from tri- stereo Pleiades- 1 satellite imagery for lava flow volume estimates at Fogo Volcano.

Geophysical Research Letters, 43(12), 6267-6275.

Barberi, F., Rosi, M., Sodi, A. (1993). Volcanic hazard assessment at Stromboli based on review of historical data. Acta Vulcanologica, 3, 173-187.

Bonaccorso, A., Calvari, S., Garfì, G., Lodato, L., & Patanè, D. (2003). Dynamics of the December 2002 flank failure and tsunami at Stromboli volcano inferred by volcanological and geophysical observations. Geophysical Research Letters, 30(19).

Bosman, A., Casalbore, D., Romagnoli, C., & Chiocci, F. L. (2014). Formation of an 'a'ā lava delta: insights from time-lapse multibeam bathymetry and direct observations during the Stromboli 2007 eruption. Bulletin of Volcanology, 76(7), 1-12.

Calvari, S., Di Traglia, F., Ganci, G., Giudicepietro, F., Macedonio, G., Cappello, A., Nolesini, Pecora, E., Bilotta, G., Centorrino, V., Corradino, C., Casagli, N., & Del Negro, C. (2020). Overflows and pyroclastic density currents in March-April 2020 at Stromboli volcano detected by remote sensing and seismic monitoring data. Remote Sensing, 12(18), 3010.

Calvari, S., Giudicepietro, F., Di Traglia, F., Bonaccorso, A., Macedonio, G., & Casagli, N. (2021). Variable Magnitude and Intensity of Strombolian Explosions: Focus on the Eruptive Processes for a First Classification Scheme for Stromboli Volcano (Italy). Remote Sensing, 13(5), 944.

Casalbore, D., Romagnoli, C., Chiocci, F., & Frezza, V. (2010). Morpho-sedimentary characteristics of the volcaniclastic apron around Stromboli volcano (Italy). Marine Geology, 269(3-4), 132-148.

Casalbore, D., Passeri, F., Tommasi, P., Verrucci, L., Bosman, A., Romagnoli, C., & Chiocci, F. L. (2020). Small-scale slope instability on the submarine flanks of insular volcanoes: The case-study of the Sciara del Fuoco slope (Stromboli). International Journal of Earth Sciences, 109(8), 2643-2658.

Casalbore, D., Di Traglia, F., Bosman, A., Romagnoli, C., Casagli, N., & Chiocci, F. L. (2021). Submarine and Subaerial Morphological Changes Associated with the 2014 Eruption at Stromboli Island. Remote Sensing, 13(11), 2043.

Chiocci, F. L., Romagnoli, C., & Bosman, A. (2008a). Morphologic resilience and depositional processes due to the rapid evolution of the submerged Sciara del Fuoco (Stromboli Island) after the December 2002 submarine slide and tsunami. Geomorphology, 100(3-4), 356-365.

Chiocci, F. L., Romagnoli, C., Tommasi, P., & Bosman, A. (2008b). The Stromboli 2002 tsunamigenic submarine slide: characteristics and possible failure mechanisms. Journal of Geophysical Research: Solid Earth, 113(B10).

Civico, R., Ricci, T., Scarlato, P., Andronico, D., Cantarero, M., Carr, B.B., De Beni, E., Del Bello, E., Johnson, J.B., Kueppers, U., Pizzimenti, L., Schmid, M., Strehlow, K., Taddeucci, J.

Unoccupied Aircraft Systems (UASs) (2021). Reveal the Morphological Changes at Stromboli Volcano (Italy) before, between, and after the 3 July and 28 August 2019 Paroxysmal Eruptions. Remote Sensing, 13, 2870. https://doi.org/10.3390/rs13152870.

Cole PD., Calder ES, Druitt TH, Hoblitt R, Robertson R, Sparks RSJ, Young SR (1998) Pyroclastic flows generated by gravitational instability of the 1996–97 lava dome of Soufrire Hills Volcano, Montserrat. Geophys Res Lett 25(18):3425–3428

Di Traglia, F., Nolesini, T., Ciampalini, A., Solari, L., Frodella, W., Bellotti, F., Fumagalli, A., De Rosa, G. & Casagli, N. (2018). Tracking morphological changes and slope instability using spaceborne and ground-based SAR data. Geomorphology, 300, 95-112.

Di Traglia, F., Fornaciai, A., Favalli, M., Nolesini, T., & Casagli, N. (2020). Catching geomorphological response to volcanic activity on steep slope volcanoes using multi-platform remote sensing. Remote Sensing, 12(3), 438.

Esposti Ongaro, T., de'Michieli Vitturi, M., Cerminara, M., Fornaciai, A., Nannipieri, L., Favalli, M., Calusi, B., Macías, J., Castro, M.J., Ortega, S., González-Vida, J.M., Escalante, C. (2021). Modeling Tsunamis Generated by Submarine Landslides at Stromboli Volcano (Aeolian Islands, Italy): A Numerical Benchmark Study. Frontiers in Earth Science, 9, 274.

Fauria, K. E., Manga, M., & Chamberlain, M. (2016). Effect of particle entrainment on the runout of pyroclastic density currents. Journal of Geophysical Research: Solid Earth, 121(9),

6445-6461.

Favalli, M., Karátson, D., Mazzarini, F., Pareschi, M. T., & Boschi, E. (2009). Morphometry of scoria cones located on a volcano flank: a case study from Mt. Etna (Italy), based on high-resolution LiDAR data. Journal of Volcanology and Geothermal Research, 186(3-4), 320-330.

Favalli, M., Fornaciai, A., Mazzarini, F., Harris, A., Neri, M., Behncke, B., Pareschi, M. T., Tarquini, S. & Boschi, E. (2010). Evolution of an active lava flow field using a multitemporal LIDAR acquisition. Journal of Geophysical Research: Solid Earth, 115(B11).

Favalli, M., Fornaciai, A., Nannipieri, L., Harris, A., Calvari, S., & Lormand, C. (2018). UAV-based remote sensing surveys of lava flow fields: a case study from Etna's 1974 channel-fed lava flows. Bulletin of Volcanology, 80(3), 1-18.

Fornaciai, A., Favalli, M., Nannipieri, L. (2019), numerical simulation of the tsunamis generated by the Sciara del fuoco landslides (Stromboli Island, Italy), Scientific Reports 9, 18542, https://doi.org/10.1038/s41598-019-54949-7

Giordano, G., & De Astis, G. (2021). The summer 2019 basaltic Vulcanian eruptions (paroxysms) of Stromboli. Bulletin of Volcanology, 83(1), 1-27.

Giudicepietro, F., Lopez, C., Macedonio, G., Alparone, S., Bianco, F., Calvari, S., De Cesare, W., Delle Donne, D., Di Lieto, B., Esposito, A.M., Orazi, M., Peluso, R., Privitera, E., Romano,

P., Scarpato, G., Tramelli, A. (2020) Geophysical precursors of the July-August 2019 paroxysmal eruptive phase and their implications for Stromboli volcano (Italy) monitoring. Scientific Reports, 10, 10296, https://doi.org/10.1038/s41598-020-67220-1.

Hart, K., Carey, S., Sigurdsson, H., Sparks, R. S. J., & Robertson, R. E. (2004). Discharge of pyroclastic flows into the sea during the 1996–1998 eruptions of the Soufrière Hills volcano, Montserrat. Bulletin of Volcanology, 66(7), 599-614.

INGV (2019). Comunicato Straordinario Stromboli 04/07/2019. Press release n.16, Istituto Nazionale di Geofisica e Vulcanologia. http://www.ingv.it/it/stampa-e-urp/stampa/comunicati-stampa-1/2019/37-comunicato-straordinario-stromboli-04-07-2019-09-00-utc-aggiornamento-sul-fenomeno-in-corso/file

Laiolo, M., Massimetti, F., Cigolini, C., Ripepe, M., & Coppola, D. (2018). Long-term eruptive trends from space-based thermal and SO 2 emissions: a comparative analysis of Stromboli, Batu Tara and Tinakula volcanoes. Bulletin of Volcanology, 80(9), 1-19.

LGS (2019a). Esplosione parossistica del vulcano Stromboli del 03/07/2019. Report to the Italian Department of Civil Protection, Universita` di Firenze. http://lgs.geo.unifi.it/index.php/reports/comunicati?view=document&id=7:esplosione-parossistica-03-07-2019&catid=14

LGS (2019b). Esplosione parossistica del vulcano Stromboli del 28/08/2019. Report to the

Italian Department of Civil Protection, Universita` di Firenze. http://lgs.geo.unifi.it/index.php/reports/comunicati?view=document&id=8:esplosione-parossistica-28-08-2019&catid=14

Lodato, L., Spampinato, L., Harris, A., Calvari, S., Dehn, J., & Patrick, M. (2007). The morphology and evolution of the Stromboli 2002–2003 lava flow field: an example of a basaltic flow field emplaced on a steep slope. Bulletin of volcanology, 69(6), 661-679.

Maeno, F., & Imamura, F. (2007). Numerical investigations of tsunamis generated by pyroclastic flows from the Kikai caldera, Japan. Geophysical Research Letters, 34(23).

Maramai, A., Graziani, L., & Tinti, S. (2005). Tsunamis in the Aeolian Islands (southern Italy): a review. Marine Geology, 215(1-2), 11-21.

Marsella, M., Baldi, P., Coltelli, M., & Fabris, M. (2012). The morphological evolution of the Sciara del Fuoco since 1868: Reconstructing the effusive activity at Stromboli volcano. Bulletin of Volcanology, 74(1), 231-248.

McCoy, F. W., & Heiken, G. (2000). Tsunami generated by the Late Bronze age eruption of Thera (Santorini), Greece. Pure and Applied Geophysics, 157(6), 1227-1256.

Németh, K., & Martin, U. (2007). Practical Volcanology, Occasional Papers of the Geological Institute of Hungary. Budapest, 207, 1-221.

Nolesini, T., Di Traglia, F., Del Ventisette, C., Moretti, S., & Casagli, N. (2013). Deformations and slope instability on Stromboli volcano: Integration of GBInSAR data and analog modeling. Geomorphology, 180, 242-254.

Kokelaar, P., & Romagnoli, C. (1995). Sector collapse, sedimentation and clast population evolution at an active island-arc volcano: Stromboli, Italy. Bulletin of Volcanology, 57(4), 240-262

Plank, S., Marchese, F., Filizzola, C., Pergola, N., Neri, M., Nolde, M., & Martinis, S. (2019). The July/August 2019 Lava Flows at the Sciara del Fuoco, Stromboli–Analysis from Multi-Sensor Infrared Satellite Imagery. Remote Sensing, 11(23), 2879.

Pollock, N. M., Brand, B. D., & Roche, O. (2016). The controls and consequences of substrate entrainment by pyroclastic density currents at Mount St Helens, Washington (USA). Journal of Volcanology and Geothermal Research, 325, 135-147.

Roche, O. (2015). Nature and velocity of pyroclastic density currents inferred from models of entrainment of substrate lithic clasts. Earth and Planetary Science Letters, 418, 115-125.

Romagnoli, C., Casalbore, D., Chiocci, F. L., & Bosman, A. (2009). Offshore evidence of large-scale lateral collapses on the eastern flank of Stromboli, Italy, due to structurally-controlled, bilateral flank instability. Marine Geology, 262(1-4), 1-13.

Rosi, M., Pistolesi, M., Bertagnini, A., Landi, P., Pompilio, M., & Di Roberto, A. (2013). Stromboli volcano, Aeolian Islands (Italy): present eruptive activity and hazards. Geological Society, London, Memoirs, 37(1), 473-490.

Roverato, M., Di Traglia, F., Procter, J., Paguican, E., & Dufresne, A. (2021). Factors contributing to volcano lateral collapse. In Volcanic Debris Avalanches (pp. 91-119). Springer, Cham.

Shimizu, H. A., Koyaguchi, T., & Suzuki, Y. J. (2019). The run-out distance of large-scale pyroclastic density currents: a two-layer depth-averaged model. Journal of Volcanology and Geothermal Research, 381, 168-184.

Sassa, K., & hui Wang, G. (2005). Mechanism of landslide-triggered debris flows: Liquefaction phenomena due to the undrained loading of torrent deposits. In Debris-flow hazards and related phenomena (pp. 81-104). Springer, Berlin, Heidelberg.

Smellie JL, Wilch TI, Rocchi S (2013) 'A'ā lava-fed deltas: a new reference tool in paleoenvironmental studies. Geology 41:403–406. doi:10.1130/G33631.1

Soule, S. A., Zoeller, M., & Parcheta, C. (2021). Submarine lava deltas of the 2018 eruption of Kīlauea volcano. Bulletin of Volcanology, 83(4), 1-16.

Spina, L., Del Bello, E., Ricci, T., Taddeucci, J., & Scarlato, P. (2021). Multi-parametric characterization of explosive activity at Batu Tara Volcano (Flores Sea, Indonesia). Journal of Volcanology and Geothermal Research, 413, 107199.

Thouret, J. C. (1999). Volcanic geomorphology—an overview. Earth-science reviews, 47(1-2), 95-131.

Tinti, S., Manucci, A., Pagnoni, G., Armigliato, A., & Zaniboni, F. (2005). The 30 December 2002 landslide-induced tsunamis in Stromboli: sequence of the events reconstructed from the eyewitness accounts. Natural Hazards and Earth System Sciences, 5(6), 763-775.

Tinti, S., Pagnoni, G., & Zaniboni, F. (2006). The landslides and tsunamis of the 30th of December 2002 in Stromboli analysed through numerical simulations. Bulletin of Volcanology, 68(5), 462-479.

Turchi, A., Di Traglia, F., Luti, T., Olori, D., Zetti, I., & Fanti, R. (2020). Environmental aftermath of the 2019 Stromboli Eruption. Remote Sensing, 12(6), 994.

Verrucci, L., Tommasi, P., Boldini, D., Graziani, A., & Rotonda, T. (2019). Modelling the instability phenomena on the NW flank of Stromboli Volcano (Italy) due to lateral dyke intrusion. Journal of Volcanology and Geothermal Research, 371, 245-262.

Ward, S. N. (2001). Landslide tsunami. Journal of Geophysical Research: Solid Earth, 106(B6),

11201-11215.

Author Contributions

Federico Di Traglia: conception and realization of the manuscript, data analysis, field validation (fditraglia@inogs.it) [corresponding author]

Alessandro Fornaciai: conception and realization of the manuscript, data analysis (alessandro.fornaciai@ingv.it)

Daniele Casalbore: conception and realization of the manuscript, data analysis, field validation (daniele.casalbore@uniroma1.it)

Massimiliano Favalli: realization of the manuscript, data analysis (massimiliano.favalli@ingv.it)

Irene Manzella: realization of the manuscript, financial support (irene.manzella@plymouth.ac.uk)

Claudia Romagnoli: realization of the manuscript, data analysis (claudia.romagnoli@unibo.it)

Francesco Latino Chiocci: realization of the manuscript, data analysis, financial support (francesco.chiocci@uniroma1.it)

Paul Cole: realization of the manuscript (paul.cole@plymouth.ac.uk)

Teresa Nolesini: realization of the manuscript, data analysis, field validation (teresa.nolesini@unifi.it)

Nicola Casagli: realization of the manuscript, financial support (nicola.casagli@unifi.it)

Funding

This research was funded by the "Presidenza del Consiglio dei Ministri–Dipartimento della Protezione Civile" (Presidency of the Council of Ministers–Department of Civil Protection), through the UniFi-DPC 2019-2021 agreement (Scientific Responsibility: N.C.). The contents of this paper represent the authors' ideas and do not necessarily correspond to the official opinion and policies of the "Presidenza del Consiglio dei Ministri–Dipartimento della Protezione Civile" (Presidency of the Council of Ministers–Department of Civil Protection).

This research was also funded by the NERC Project "Tsunamigenic mass flows at Stromboli Volcano-analysis and modelling after the 3rd of July events" (NE/T009438/1; Scientific Responsibility: I.M.)

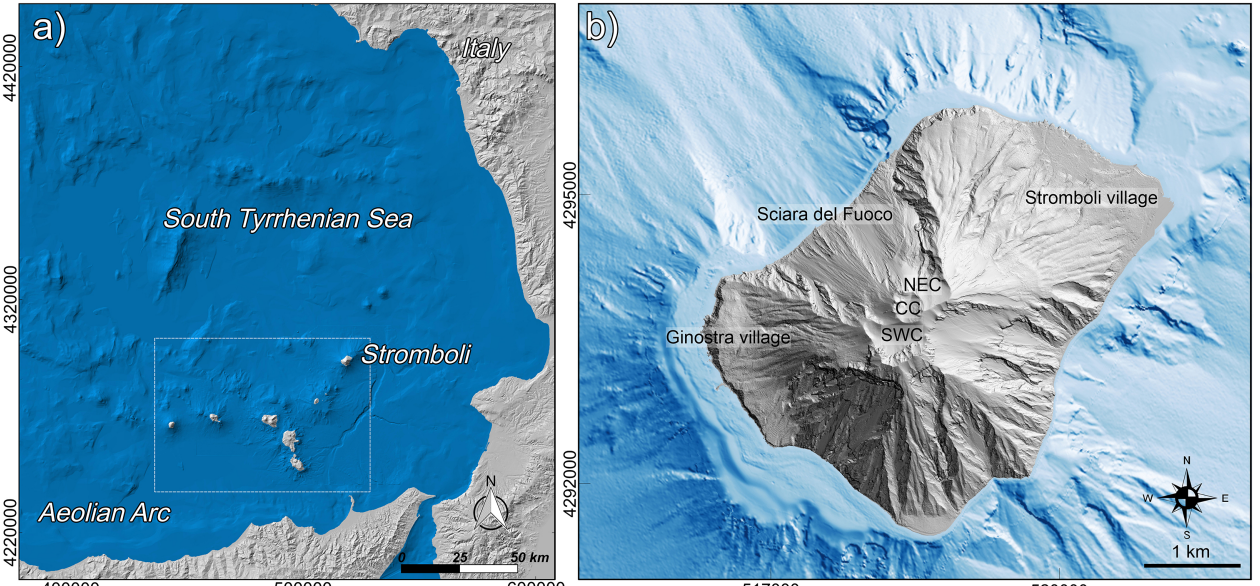
a)
Italy
South Tyrrhenian Sea
Stromboli
Aeolian Arc
N
0 25 50 km
4420000
4320000
4220000
400000
500000
600000
b)
Sciara del Fuoco
Stromboli village
NEC
CC
SWC
Ginostra village
N
W
E
S
1 km
4295000
4292000
517000
520000

Figure 1

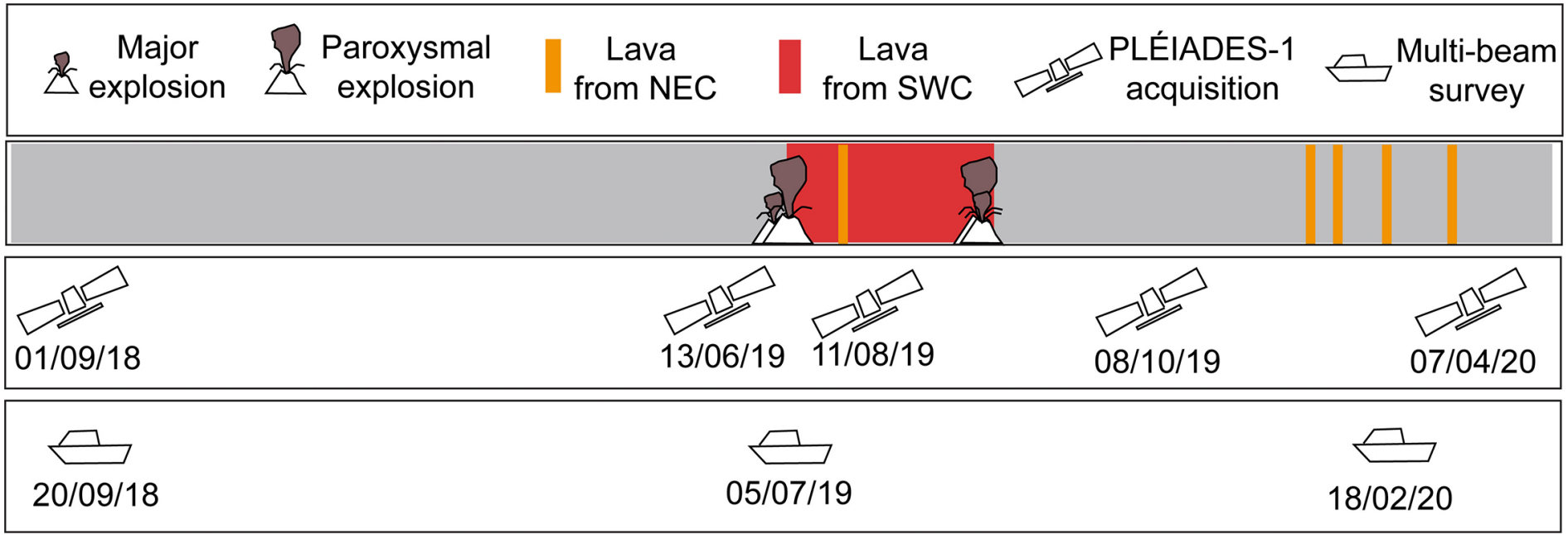
Major explosion
Paroxysmal explosion
Lava from NEC
Lava from SWC
PLÉIADES-1 acquisition
Multi-beam survey
01/09/18
13/06/19
11/08/19
08/10/19
07/04/20
20/09/18
05/07/19
18/02/20

Figure 2

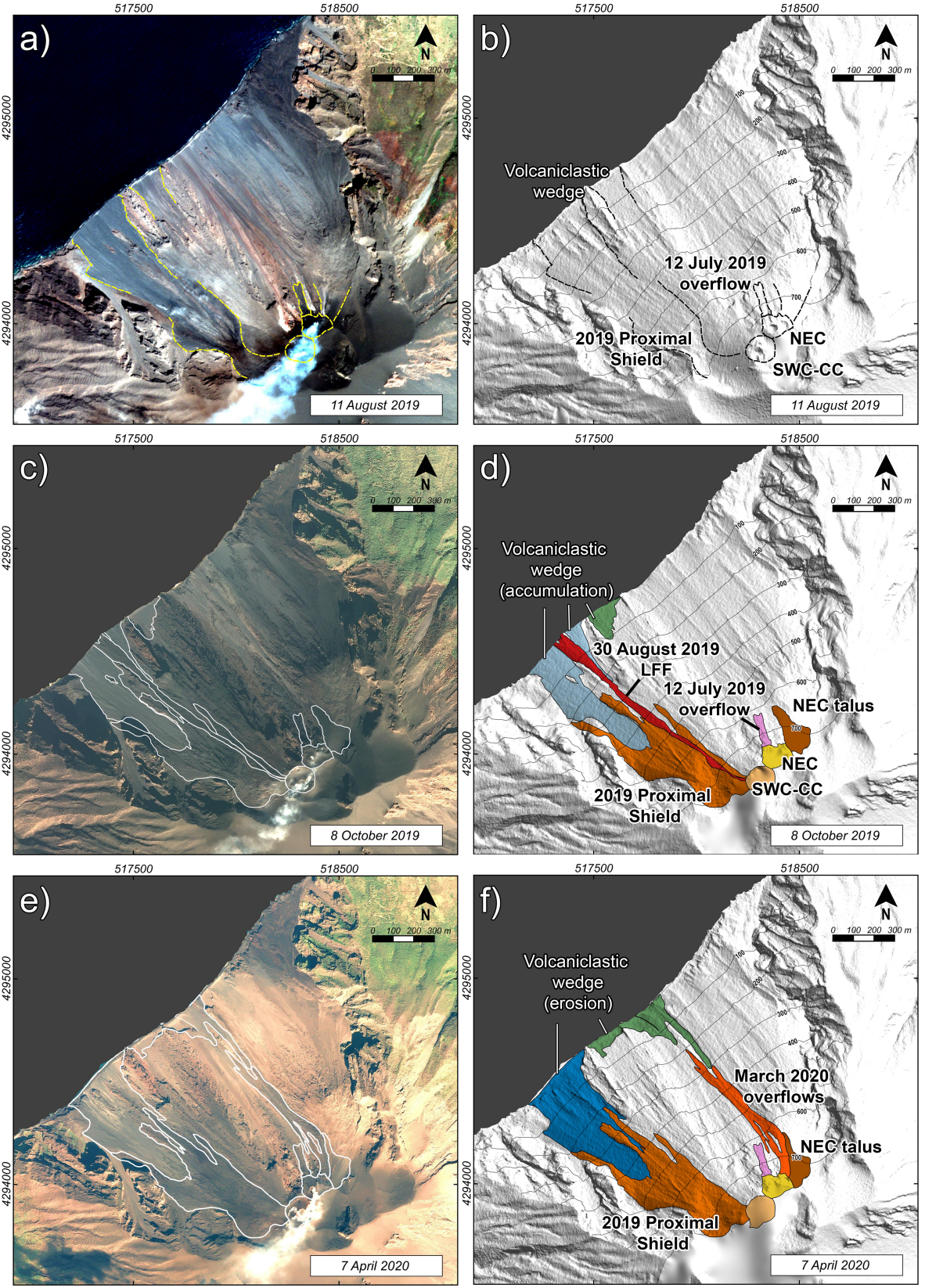
a)
b)
c)
d)
e)
f)
517500
518500
4295000
4294000
N
0 100 200 300 m
Volcaniclastic wedge
12 July 2019 overflow
2019 Proximal Shield
NEC
SWC-CC
11 August 2019
Volcaniclastic wedge (accumulation)
30 August 2019 LFF
NEC talus
8 October 2019
Volcaniclastic wedge (erosion)
March 2020 overflows
7 April 2020

Figure 3

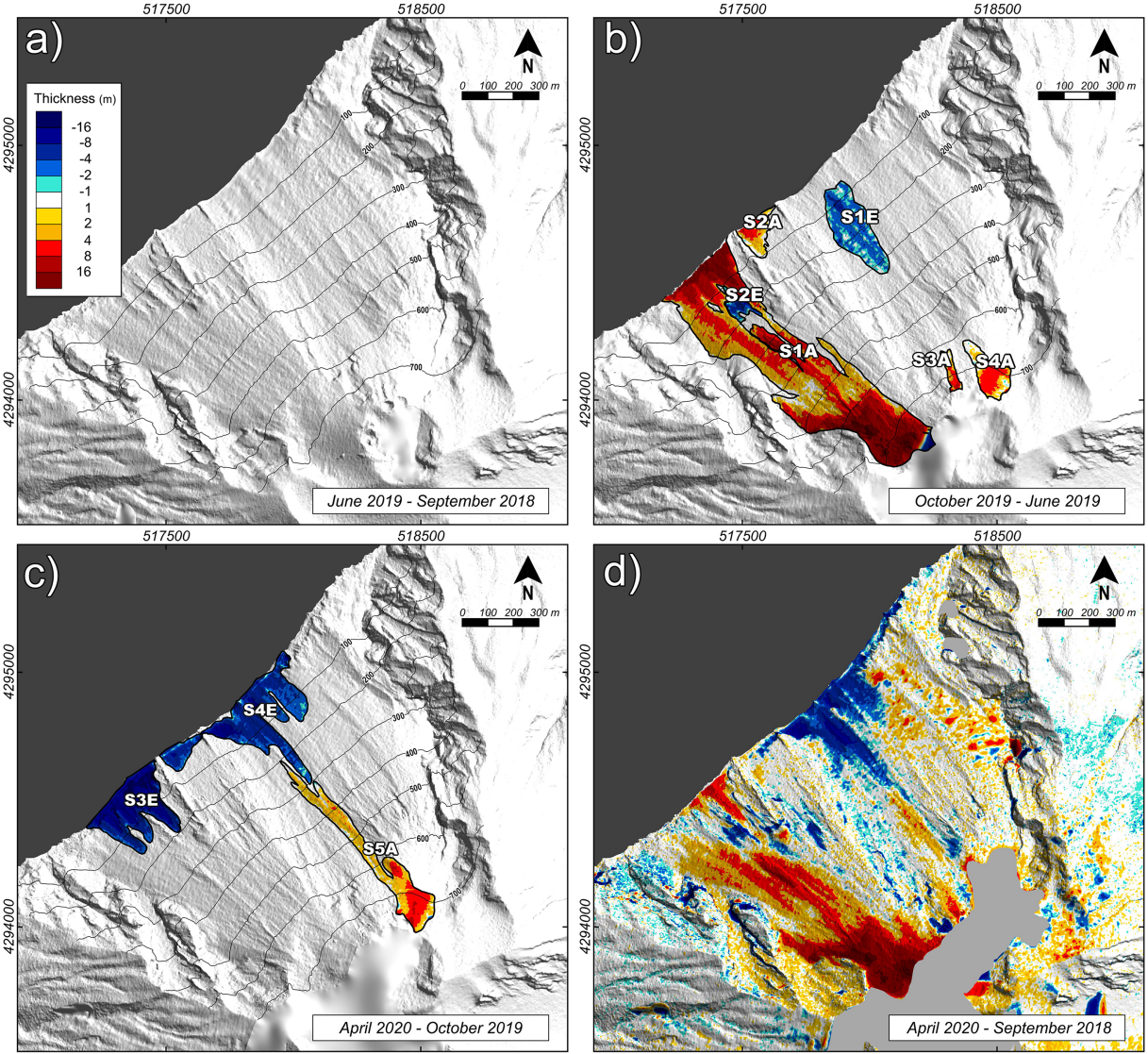
a)
Thickness (m)
-16
-8
-4
-2
-1
1
2
4
8
16
June 2019 - September 2018
b)
S2A
S1E
S2E
S1A
S3A
S4A
October 2019 - June 2019
c)
S4E
S3E
S5A
April 2020 - October 2019
d)
April 2020 - September 2018
517500
518500
4295000
4294000
N
0 100 200 300 m

Figure 4

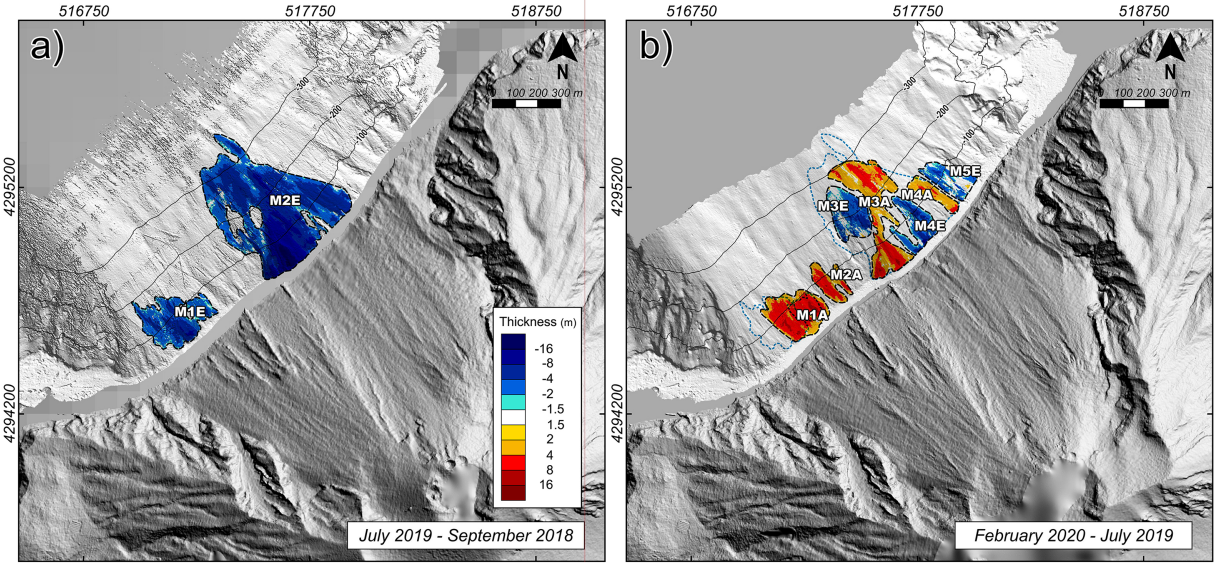
a)
b)
516750
517750
518750
4295200
4294200
N
100 200 300 m
M1E
M2E
M1A
M2A
M3E
M3A
M4A
M4E
M5E
Thickness (m)
-16
-8
-4
-2
-1.5
1.5
2
4
8
16
July 2019 - September 2018
February 2020 - July 2019

Figure 5

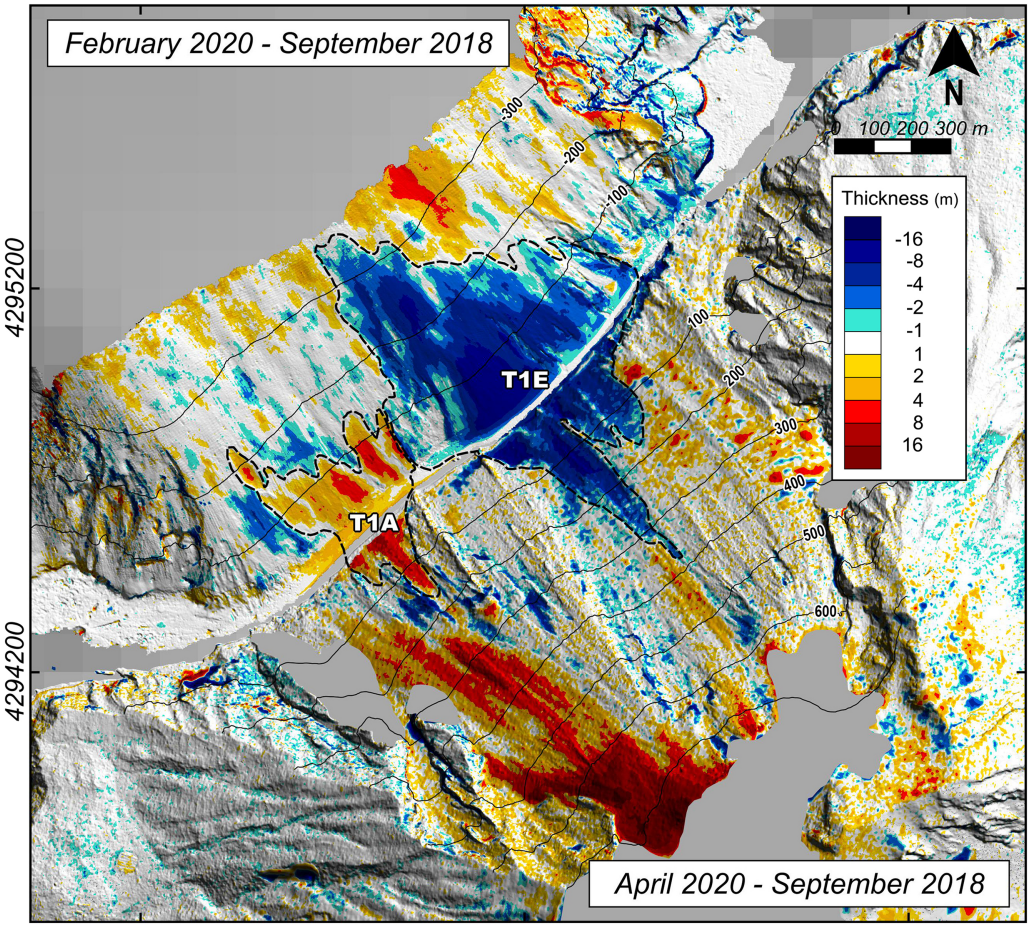
516750
517750
518750
February 2020 - September 2018
N
0 100 200 300 m
Thickness (m)
-16
-8
-4
-2
-1
1
2
4
8
16
T1E
T1A
4295200
4294200
April 2020 - September 2018

Figure 6